Research Article

El-Sayed M. Sherif*

Beneficial effect of 4% Ta addition on the corrosion mitigation of Ti–12% Zr alloy after different immersion times in 3.5% NaCl solutions

https://doi.org/10.1515/secm-2024-0016
received March 13, 2024; accepted April 22, 2024

Abstract: The recent study reports the fabrication and corrosion behavior of two Ti alloys, 88% Ti–12% Zr and 84% Ti–12% Zr–4% Ta, in 3.5% NaCl electrolyte. These alloys were manufactured using powder metallurgy, where the powders were mixed, ball milled, and sintered. The corrosion behavior of these alloys was examined using various electrochemical and spectroscopic tests. Cyclic polarization experiments indicated that adding 4% Ta reduces corrosion of the TiZr alloy by suppressing anodic dissolution, resulting in a lower corrosion rate. The Nyquist and Bode impedance spectra for the tested alloys revealed that the presence of 4% Ta within TiZr alloy highly decreases the corrosion by increasing the impedance of the interface, the maximum degree of phase angle, and polarization resistance. The chronoamperometric current measured at −0.10 V (Ag/AgCl) proved that the presence of 4% Ta powerfully alleviates both uniform and pitting corrosion for TiZr alloy by lowering the obtained absolute currents. The surface investigation using scanning electron microscopy confirmed the homogeneity of the surfaces. The elemental analysis performed on the surface using energy dispersive spectroscopy revealed that the surface of TiZr alloy forms a top film including different oxides such as TiO_2 and ZrO_2, and for TiZrTa alloy, the surface has TiO_2 + ZrO_2 plus TaO_2. Experiments demonstrated that Ta has the ability to increase the corrosion passivation of TiZr alloy.

Keywords: Ti-base alloys, Ta addition, corrosion passivation, electrochemical techniques, surface morphology

1 Introduction

Ti-base alloys have unique characteristics that make them suitable for a wide range of applications [1–3], including in the biomedical field, automotive main and spare parts, aerospace industries, *etc.* [4–7]. Ti-base alloys are distinguished by their superior biocompatibility and biodegradability, great corrosion resistance, and exceptional mechanical and tribological properties. Several scientists [7–9] have reported the use of titanium aluminum vanadium (Ti6Al4V) alloy as a biomedical material in the replacement of fractured bones, tissue repair, and transplantation procedures in the human bodies. Conversely, some side effects were found while using Ti6Al4V alloy in the human body [8–12]. It was reported that the alloy contains Al and V, which react with the medium in which it is implanted, releasing toxic radicals of Al^{3+} and V^{5+}. When these active species are released into the patients' bloodstreams, they trigger hazardous reactions and may increase the risk of Alzheimer's disease [13–15].

Regardless of research and development efforts in the field of artificial tissues for human bodies, there is a need for developing new alloys and composites to overcome the shortcomings of the currently used materials. Several trials have been conducted to avoid the presence of active radicals such as the toxic Al^{3+} and V^{5+} cations [16,17]. Wu *et al.* developed Ti–12Nb–12Zr–12Sn alloy using the machine learning method, namely, an artificial neural network [18]. The addition of Zr to form various Zr percentages of Ti–*x*Zr alloys has been reported by numerous researchers [17–21]. The binary has the same α structure as commercially pure Ti (cp Ti) and is highly compatible with biological fluids [19]. This is because Ti–Zr binary is considered an ideal implant material due to its high resistance to corrosion resistance, outstanding mechanical properties, exceptional biocompatibility, strength, and osseointegration characteristics [21].

It was found that adding 15% Zr to pure Ti enhances corrosion resistance when exposed to simulated body fluid (SBF), and that this effect significantly magnifies the

* **Corresponding author: El-Sayed M. Sherif**, Mechanical Engineering Department, College of Engineering, King Saud University, P.O. Box 800, Al-Riyadh, 11421, Saudi Arabia, e-mail: esherif@ksu.edu.sa

mechanical characteristics of Ti [1]. The effect of adding Zr and Ta to pure Ti, 15% Zr + 2% Ta, has also been reported [2], and it was found to significantly improve the corrosion resistance as compared to Ti and the Ti15% Zr alloy. The addition of Zr and Ta to Ti not only enhances corrosion resistance in SBF solution but also strongly increases the hardness of the alloy [22]. The high corrosion resistance of many Ti-base alloys is due to the development of an oxide (TiO_2) film [23–25]. For example, TiZr and TiZrTa, TiAlV alloys, it forms not only TiO_2 but also other oxides such as ZrO_2, TaO_2, and VO_2 that highly increase their passivation [1,2,26].

The implantation of Zr, Ta, and other alloying elements with Ti, such as Hf, Nb, Sn, and so on, has been investigated to produce different series of alloys from TiZrTaHf and TiTaNbZr [20,26–32]. The current research aims at the fabrication of two alloys with the following compositions: 88% Ti–12% Zr alloy and 84% Ti–12% Zr–4% Ta alloy. The corrosion of these alloys in solution (3.5% NaCl) was tested after two exposure periods of 30 min and 3 days at room temperature. Various methods were used such as cyclic polarization, impedance spectroscopy, and chronoamperometric currents vs. time. Surface investigations were carried out using scanning electron microscopy (SEM) and energy dispersive spectroscopy (EDS) analyses.

2 Materials and methods

Pure sodium chloride (NaCl, 99.9 purity) was supplied by Merck. To make a liter of 3.5% NaCl solution, weigh 35 g of the NaCl salt and dissolve it in distilled water. A 99.9% pure Ti powder, 99% pure Zr powder, and 99.9% pure Ta were used as received. The particle size of the powders is 5–7, 10, and 10 μm for Ti, Zr, and Ta, respectively. All these powders were obtained from Nanochemazone, Leduc, Alberta, Canada. Different powders were weighed to the desired weight and mixed in a ball mill (high energy). The weighed powders and balls (ball-to-powder ratio was 90:10) were mixed at 150 rpm for 30 min. The mixtures of powders were placed in graphite dies and sintered in a high-frequency heat induction furnace following the procedures described in the earlier studies [1,2].

For corrosion testing, the TiZr alloy and TiZrTa alloy electrodes were welded onto one face using copper wire. The electrodes were placed in an electrically inert epoxy resin. The other face of the mounted electrode was ground with emery sheets of various grits up to 1,000. The corrosion tests were conducted using a three-electrode electrochemical cell with a solution capacity of 60 mL. The three electrodes were the fabricated alloys, Ag/AgCl, and a platinum sheet, which served as the working, reference, and counter, respectively. The Metrohm Autolab model PGSTAT302N was used.

The cyclic polarization plots were obtained from −970 mV to +170 mV, starting from the forward potential, then in the backward directions, and back again at a scan rate of 0.1667 mV/s. The spectra of electrochemical impedance spectroscopy (EIS) were recorded at the steady potential values ranging from 100 kHz to 100 mHz as the scanning frequency. The EIS points were collected using Powersine software, with a point rate of 10 for every decade variation in frequency. ZSimpWin v.3.1 software was used to fit the EIS data. Chronoamperometric curves were collected at fixed voltage of −100 mV for 30 min. The morphology of the surface was investigated using a JEOL model JSM-7400F SEM (Tokyo, Japan). An attached unit of EDS was used to report the compositions of the surface produced film(s).

3 Results and discussion

3.1 Cyclic potentiodynamic polarization (CPP)

Figure 1 shows the CPP curves for (1) TiZr alloy and (2) TiZrTa alloy after immersion in 3.5% NaCl solution for 30 min. The CPP method has been widely recognized as the most successful technique for reporting corrosion parameters; besides, it can provide information on the occurrence and intensity of pitting corrosion [1,2,8,33–35]. To report the effect of longer immersion times, measurements were repeated for the same alloys after 3 day, as shown in

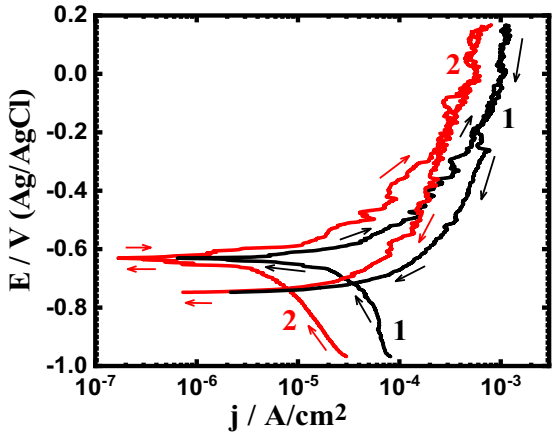

Figure 1: CPP curves for (1) TiZr alloy and (2) TiZrTa alloy after 30 min exposure to the NaCl solutions.

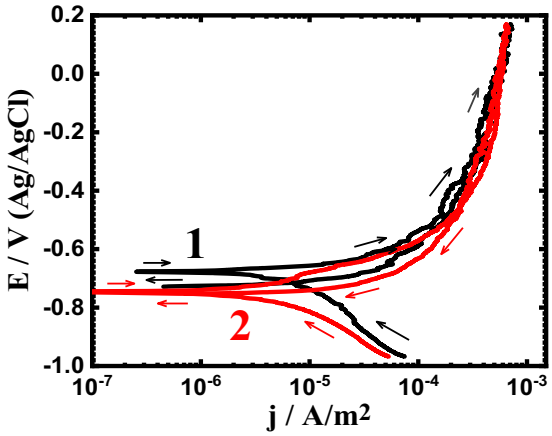

Figure 2: CPP curves for (1) TiZr alloy and (2) TiZrTa alloy in NaCl solutions for 3 days.

Figure 2. The polarization curves were used to obtain the corrosion parameters listed in Table 1. The extrapolated tangents to the linearized cathodic and anodic current regions were used to calculate the values of the cathodic (β_c) and anodic (β_a) Tafel slopes, respectively. Other values for E_{Corr}, corrosion potential, and j_{Corr}, corrosion current, were reported in previous studies [33–35]. The values of corrosion rate (R_{Corr}) and polarization resistance (R_P) were obtained as follows [33–35]:

$$R_P = \frac{1}{j_{Corr}}\left(\frac{\beta_c \cdot \beta_a}{2.3(\beta_c + \beta_a)}\right), \quad (1)$$

$$R_{Corr} = j_{Corr}\left(\frac{k \cdot E_W}{d \cdot A}\right), \quad (2)$$

where k is a constant that defines the unit of corrosion rate, k = 3,272 mm (amp/cm/year), E_W is the equivalent weight, d is the density, and A is the area. It is worth mentioning that the density of both 88Ti–12Zr alloy and 88Ti–12Zr–4Ta alloy was calculated to be 4.672 and 4.818 g/cm^3, respectively. The relative densities for both 88Ti–12Zr alloy and 88Ti–12Zr–4Ta alloy were 99.42 and 97.86%, respectively.

The cathodic branch for all alloys starts with a decrease in current as a result of oxygen reduction. This reaction can be expressed as follows [32,33]:

$$2H_2O + O_2 + 4e^- = 4OH^-. \quad (3)$$

The current continues to decrease till it reaches the j_{Corr} value. Then, the anodic reaction starts, which is known to be a dissolution reaction that might lead to the increase of current. Figure 1 shows that both cathodic and anodic currents for TiZr alloy (curve 1) have higher currents; these currents are highly reduced for TiZrTa alloy (curve 2). The increase of currents for both TiZr and TiZrTa alloys is expected due to the increased application of potential. The higher recorded currents for TiZr alloy as compared to the ones obtained for TiZrTa alloy is due to the presence of Ta, which allows the formation of TaO_2 in addition to the formation of TiO_2 and ZrO_2 that could also present on the surface of TiZr alloy. Table 1 also confirmed that where the value of j_{Corr} (and in accordance R_{Corr}) was higher, as well as the R_P value was lower for TiZr alloy. Moreover, the value of E_{Corr} was always less negative for TiZrTa alloy than for TiZr alloy, indicating that the presence of Ta passivates the anodic reactions more than cathodic ones.

Figure 2 shows the polarization behavior of the tested alloys after extending the immersion time in NaCl solution to 3 days, which is nearly identical. The currents (cathodic and anodic) recorded lower values for TiZrTa alloy than the values for TiZr alloy. This was also reflected in j_{Corr}, R_P, and R_{Corr}, with TiZrTa alloy having lower j_{Corr} and R_{Corr} values but a larger R_P value. The presence of Ta increases the corrosion passivation of TiZr alloy. The effect of increasing immersion duration from 30 min to 3 day can be elucidated by comparing Figures 1 and 2, as well as the values listed in Table 1. The tested alloys showed decreased anodic and cathodic currents *versus* potential after 3 days of immersion in NaCl solution, compared to their values after 30 min. The j_{Corr} and R_{Corr} for TiZr alloy measured lower values after 3 days of immersion, whereas TiZrTa alloy recorded even lower values after 3 days of immersion. The values of R_P in turn scored higher values for both alloys when the time of exposure was extended to 3 days. Prolonging the immersion time has a positive effect on the passivation of TiZr alloy and TiZrTa alloy by the formation and thickening of a mixture of oxide film(s) of TiO_2, ZrO_2, and TaO_2.

Table 1: Values obtained from CPP measurements

Alloy/time	β_c (mV/dec)	E_{Corr} (mV)	β_a (mV/dec)	j_{Corr} (μA/cm^2)	R_P (kΩ/cm^2)	R_{Corr} (mm/y)
TiZr alloy/30 min	165	−735	188	6.5	5.88	0.0643
TiZrTa alloy/30 min	170	−647	190	3.2	12.2	0.0328
TiZr alloy/3 days	190	−632	180	5.5	7.31	0.0544
TiZrTa alloy/3 days	192	−745	184	2.7	15.1	0.0277

3.2 Chronoamperometry

The chronoamperometric current *versus* time at an anodic potential technique is effective for analyzing corrosion, particularly pitting, in most active metallic materials in aggressive media [36–40]. Figure 3 shows the change in current for 30 min at −0.1 V for (1) TiZr and (2) TiZrTa alloys in NaCl solutions. Figure 3 displays that the current begins with low values and rapidly increases in the first few seconds. This results from the dissolution of a formed surface oxide film during the immersion of the alloys, which is caused by the aggressive action of the chloride solution along with the applied active voltage. It is seen from Figure 3 (curve 1) that the obtained current for TiZr alloy is the highest, where it is abruptly shifted to the higher values and then slightly increased with time. The current fluctuates up and down with an average value of 750 μA/cm^2. The increase and then the decrease in the currents result from the dissolution and subsequent formation of oxide(s), and it may also indicate pitting corrosion. TiZrTa alloy performs similarly, where the current started with an abrupt increase followed by a gradual decrease. The overall absolute currents obtained for TiZrTa alloy were far lower than those collected for TiZr alloy. This difference in the absolute currents between the two alloys results from the presence of 4% Ta, which forms an additional TaO_2 film. The formation of this oxide, along with the formation of TiO_2 and ZrO_2, passivates the surface further, which is more than the case in TiZr alloy [1,2,40].

Figure 4 shows the trends for (1) TiZr alloy and (2) TiZrTa alloy after their exposure to 3.5% NaCl solution for 3 days. The currents increased significantly in the first 30 s due to surface integration caused by the immersion of the alloys for 3 days. Here, the recorded currents for TiZr alloy show an increase followed by a decrease, with an increase in overall currents until the end of the run. The measured current for TiZrTa alloy decreased significantly

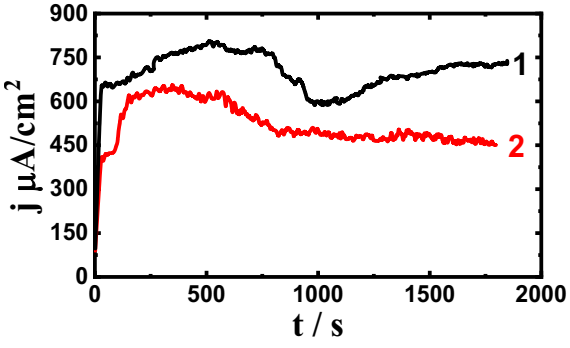

Figure 3: Current recorded at −0.1 V for (1) TiZr alloy and (2) TiZrTa alloy exposed to NaCl solutions for 30 min.

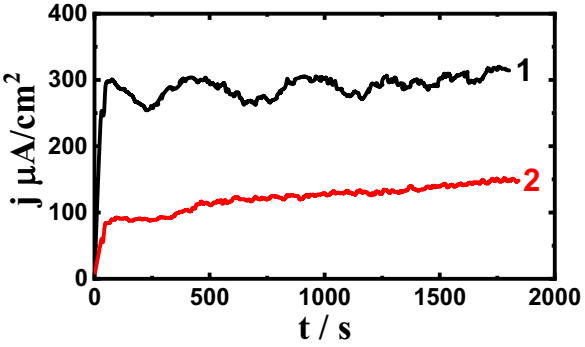

Figure 4: Current recorded at −0.1 V for (1) TiZr alloy and (2) TiZrTa exposed to NaCl solutions for 3 days.

with a gradual increase over time. This confirms the efficiency of adding Ta to TiZr alloy in reducing absolute current values, indicating a large passivation of the alloy by Ta. After 3 days of immersion in the solution (Figure 3), the current values decreased from ~750 to ~300 μA/cm^2 in the case of TiZr alloy and from ~450 to ~150 μA/cm^2 in the case of TiZrTa alloy. This is because of the formation of a thick layer of TiO_2 and ZrO_2 in the case of TiZr alloy, and TiO_2, ZrO_2, and TaO_2 for TiZrTa alloy due to the long period of exposure before applying the active potential, −0.1 V [2,40].

3.3 Surface investigation

To support corrosion experiments, the surfaces of TiZr and TiZrTa alloys were investigated using SEM after being exposed to 3.5% NaCl solutions for 3 days before stepping a potential of −0.1 V for 30 min. EDS was used to analyze the compositions of the layer(s) formed on those surfaces under the same conditions. Figure 5 presents the SEM image and EDS profile for the TiZr alloy surface following the experiments shown in Figure 4, curve 1. It clearly visualized that the surface is homogeneous and does not have shallow or deep pits. The EDS profile analysis shows that the surface contains 68.03 wt% Ti, 21.78 wt% O, and 10.19 wt% Zr. The presence of a lower percentage of Ti than its original percent, 88%, indicates that the alloy surface is covered with a film that reduces the percentage of Ti. Also, the presence of a high percentage of O, 21.78, and 10.19% Zr gives an indication that the surface of the alloy is covered with TiO_2 and ZrO_2 layer(s). The presence of such kind of oxides increases its corrosion resistance in the chloride solution.

Figure 6 shows the SEM image and EDS analysis of the TiZrTa alloy surface following the experiments shown in Figure 4, curve 2. The SEM image of Figure 6 shows

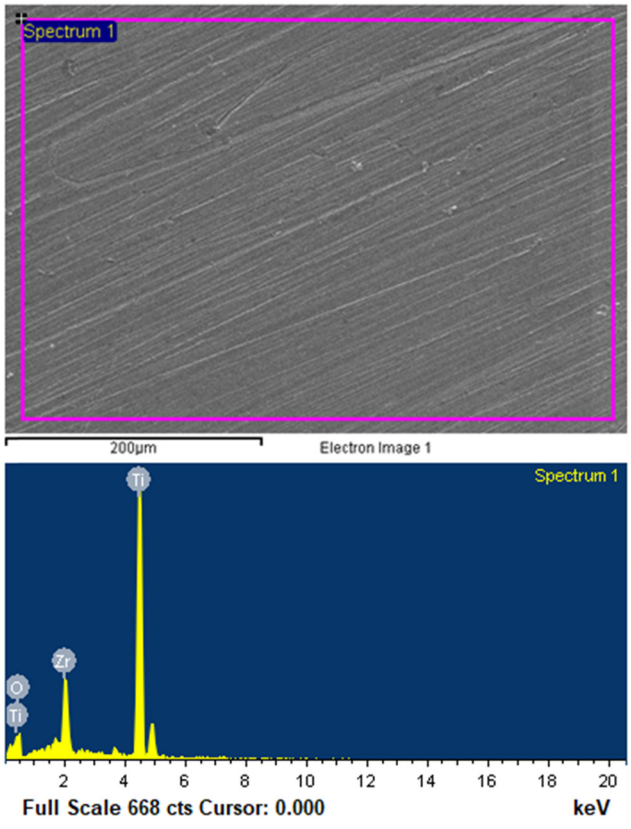

Figure 5: The SEM image and EDS analysis for the TiZr alloy surface after performing the experiments are shown in Figure 4, curve 1.

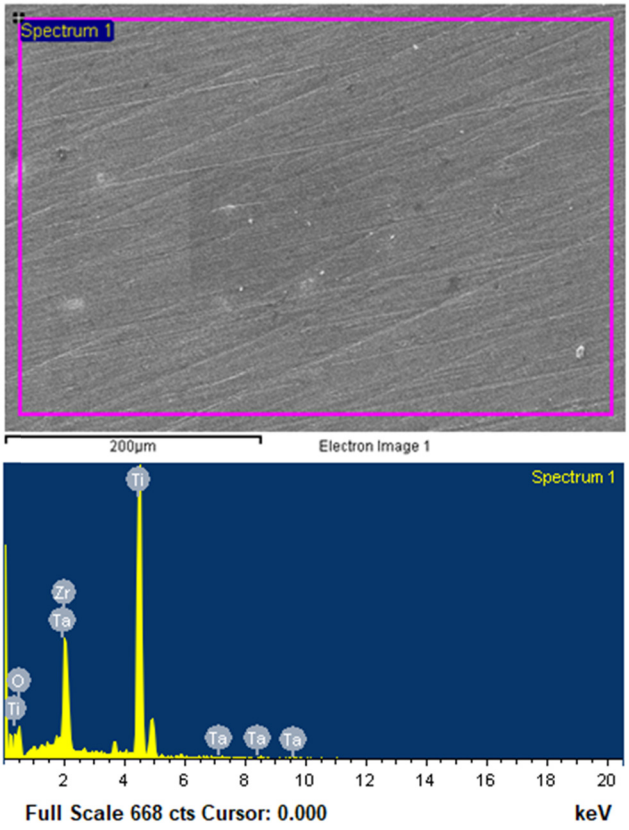

Figure 6: The SEM image and EDS analysis for the TiZrTa alloy surface after performing the experiments are shown in Figure 4, curve 2.

homogeneous surfaces with no pits. This means that a top layer formed on the surface while the alloy was immersed in the test solution. Figure 6 shows the EDS profile of the same surface, which has 64.45 wt% Ti, 24.35 wt% O, 8.86 wt% Zr, and 2.34% Ta. Again, the presence of a lower percentage of Ti, even less than the detected percentage for TiZr alloy than its original percent (88% as a starting wt%) and a high percentage of O within the surface of the alloy indicates that some oxide layer(s) cover the alloy surface. The detected weight percentages of Ti, O, Zr, and Ta indicate that the possible existing oxides on the TiZrTa alloy surface are TiO_2, ZrO_2, and TaO_2. The presence of such oxides on the surface of the alloy reveals higher corrosion passivation of the TiZrTa alloy as compared to TiZr alloy and confirms that the presence of Ta increases the corrosion passivation.

3.4 EIS

EIS has been reported to provide an important explanation for investigating the relationship between the material's interface and the test electrolyte [36–42]. The Nyquist plots for (1) TiZr alloy and (2) TiZrTa alloy after their exposure to the NaCl solutions for 30 min are shown in Figure 7. Also, the Nyquist plots were obtained for the same two alloys after being exposed to the solution for 3 days, as depicted in Figure 8. The obtained impedance results were matched to the best circuit , as shown in Figure 9. This circuit, which has varied impedance parameters, has been successfully used in numerous studies [2,40,43–47]. The elements of this model are defined as R_S is the solution resistance, Q_1 and Q_2 are constant phase elements, and R_{P1} and R_{P2} are polarization resistances. All these impedance variables with their values are listed in Table 2.

The Nyquist plots of Figure 7 exhibited one semicircle, whose diameter increased in the presence of Ta. However, the diameter obtained for TiZr is small and increases with Ta addition. This indicates that the TiZrTa alloy has improved corrosion passivation, which was confirmed by the high values of R_S, R_{P1}, and R_{P2} when compared to TiZr alloy. Q_1, Y_{Q1}, and its "n" component represent a double-layer capacitor because the value of "n" is nearly "1." The lower value of Y_{Q1} for TiZrTa alloy as compared to TiZr alloy confirms that 4% Ta significantly increases the surface corrosion passivation. This was further evidenced by

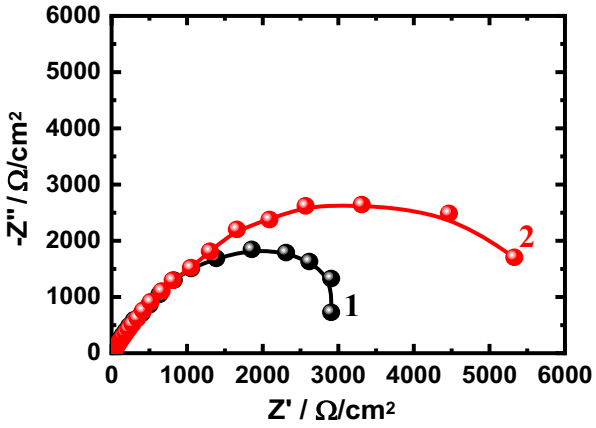

Figure 7: Nyquist plots for the (1) TiZr alloy and (2) TiZrTa alloy after their exposure to the NaCl solutions for 30 min.

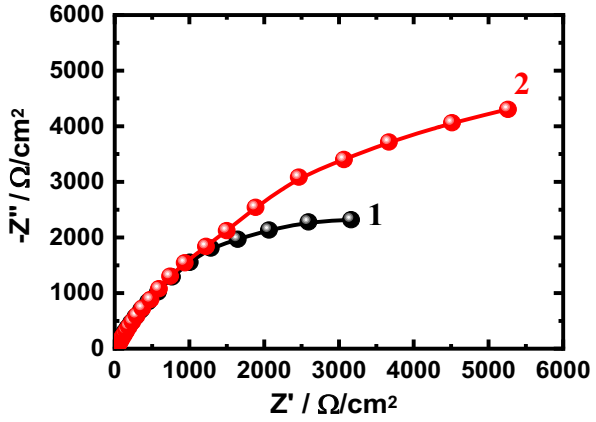

Figure 8: Nyquist plots for the (1) TiZr alloy and (2) TiZrTa alloy after their exposure to the NaCl solutions for 3 days.

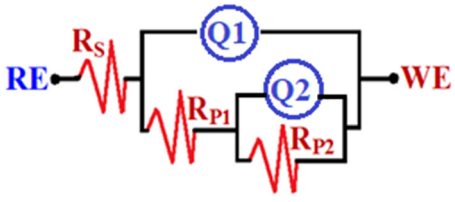

Figure 9: Circuits used to fit EIS measurements.

the presence of Q_2, which acts as a second double-layer capacitor with small pores.

Prolonging the exposure time to 3 days as shown in Figure 8 increased the size of the diameter of the semicircles obtained for TiZr alloy and TiZrTa alloy. This indicates that the corrosion passivation for both alloys improved over time, owing to the possibility for the alloys to form a protective layer, mostly oxide, which thickened with increasing immersion time. The coverage of the surfaces with this oxide(s) minimizes the ability of the corrosive chloride ions to attack the surface and thus reduces the corrosion of the alloys. Prolonging the immersion time from 30 min to 3 days highly increases the values of all resistances for both TiZr alloy and TiZrTa alloy and confirm that TiZrTa alloy has higher resistances than those obtained for TiZr alloy. As aforementioned, the presence and decrease of the values of Q_1 and Q_2, which act as double-layer capacitors, enhance the principle that extending immersion time enhances corrosion prevention. The presence of Ta in the alloy that was immersed for 3 days in NaCl solution further increases the passivation of the alloy, as confirmed by the wider semicircle (Figure 8), higher values of resistances, and lower values of the CPEs.

To support the obtained results by Nyquist plots, the Bode impedance, $|Z|$, and Bode phase angle degree, Φ, were plotted *versus* the frequency. Figure 10 shows the Bode plots for the change of $|Z|$ with frequency, which was measured for (1) TiZr alloy and (2) TiZrTa alloy in NaCl solutions after (a) 30 min and (b) 3 days, respectively. It is known that the values of $|Z|$ give important information on the corrosion of the alloys under investigation. The plots of Figure 10 show that the higher values of $|Z|$ are recorded for TiZrTa alloy, whether the immersion time is 30 min or 3 days. This indicates that alloying TiZr alloy with 4% Ta passivates the corrosion of the alloy even after 3 days of its exposure to NaCl solution before measurement.

The Bode Φ plots for the (1) TiZr alloy and (2) TiZrTa one immersed in NaCl solutions for (a) 30 min and (b) 3 days immersion are shown in Figure 11. The maximum value of Φ is always recorded for TiZrTa alloy, which

Table 2: EIS parameters obtained from the fitted EIS data

Alloy/time	R_S (Ω/cm^2)	Q_1		R_{P1} (Ω/cm^2)	Q_2		R_{P2} (Ω/cm^2)
		Y_{Q1} (F/cm^2)	n_1		Y_{Q2} (F/cm^2)	n_2	
TiZr alloy/30 min	42.4	0.00295	0.92	791	0.002864	0.89	1,089
TiZrTa alloy/30 min	48.9	0.00054	1.0	1,407	0.00216	0.77	3,702
TiZr alloy/3 days	49.7	0.00199	1.0	1,487	0.003765	0.77	1,547
TiZrTa alloy/3 days	52.1	0.00035	1.0	1,910	0.000988	0.77	4,037

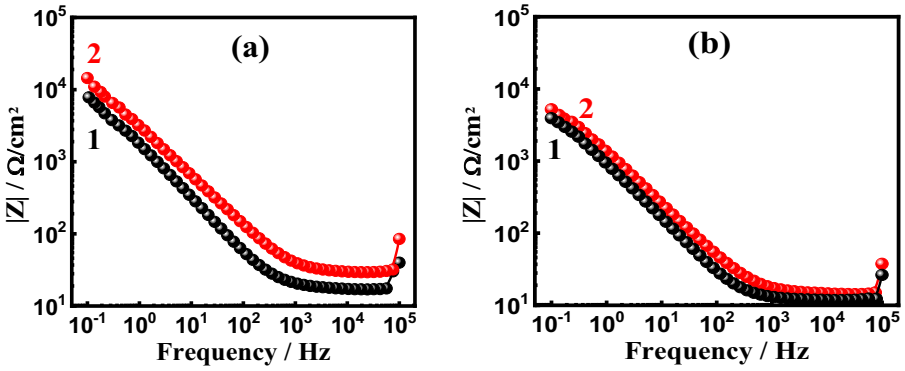

Figure 10: Bode impedance $|Z|$ for (1) TiZr and (2) TiZrTa alloys after exposure to NaCl solutions for (a) 30 min and (b) 3 days.

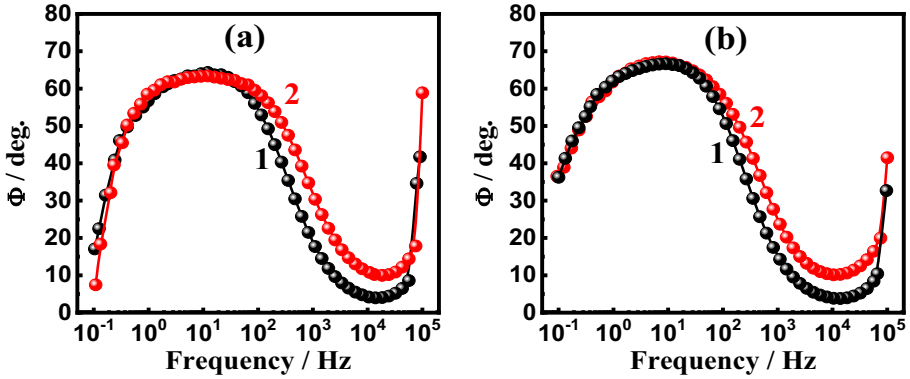

Figure 11: Bode F plots for (1) TiZr and (2) TiZrTa alloys after exposure to NaCl solutions for (a) 30 min and (b) 3 days.

confirms that the presence of Ta magnifies the resistance of TiZr alloy to corrosion both after 30-min and 3-day exposure to NaCl solution. The impedance results of both Nyquist and Bode plots thus reveal that Ta has the ability to suppress the corrosion of TiZr alloy and that the prolonging of the time of the exposure period has an additional impact on decreasing the corrosion and increasing the passivation of the test Ti-base alloy.

4 Conclusions

Two Ti alloys, Ti–12% Zr and Ti–12% Zr–4% Ta, were produced using the powder metallurgy technique. The corrosion and passivation behavior of these alloys were reported after 30 min and 3 days of exposure to 3.5% NaCl solution. Various techniques such as CPP, chronoamperometric current, and EIS were employed as electrochemical methods. After 3 days of exposure to NaCl solution, the surfaces were evaluated using SEM and EDS. The polarization, CPP, readings revealed that the addition of Ta to TiZr alloy suppresses the corrosion reactions *via* reducing the corrosion current and increases the corrosion resistance, regardless of immersion time (30 min or 3 days). The alloys were immersed for 30 min with an active anodic potential of −0.1 V. The current was measured after 3 days. Ta lowers the overall currents by increasing the corrosion resistance. SEM images and EDS profiles of the tested surfaces revealed homogenous surfaces without indication of the presence of pits. Nyquist and Bode plots confirmed CPP and chronoamperometric current experiments, which showed that the Ti alloy has increased resistances, solution, and polarization in the presence of Ta. All results also indicated that the corrosion passivation increases when prolonging the time of exposure to 3 days by thickening the formed oxides of TiO_2, ZrO_2, and TiO_2 on the alloy's top surface.

Funding information: This work was financially supported by the Researchers Supporting Project Number (RSP2024R33), King Saud University, Riyadh, Saudi Arabia.

Author contributions: The author confirms the sole responsibility for the conception of the study, presented results, and manuscript preparation.

Conflict of interest: The author states no conflict of interest.

Data availability statement: The datasets generated during and/or analyzed during the current study are available within the manuscript.

References

[1] Alharbi HF, Bahri YA, Sherif ESM. Influence of zirconium on the corrosion passivation of titanium in simulated body fluid. Crystals. 2021;11:1391. doi: 10.3390/cryst11111391.

[2] Sherif ESM, Bahri YA, Alharbi HF, Ijaz MF, Alnaser IA. Influence of tantalum addition on the corrosion passivation of titanium-zirconium alloy in simulated body fluid. Materials. 2022;15:8812. doi: 10.3390/ma15248812.

[3] Aghdam MM, Morsali SM. Effects of manufacturing environments on the residual stresses in a SiC/Ti metal-matrix composite. J Sci Eng Compos Mater. 2017;24(6):817–24. doi: 10.1515/secm-2015-0089.

[4] Sherif ESM. A comparative study on the corrosion of pure titanium and titanium-12% zirconium alloy after different exposure periods of time in sodium chloride solution. AIP Advances. 2024;14(3):035314. doi: 10.1063/5.0192701.

[5] Abdel-Hady M, Fuwa H, Hinoshita K, Kimura H, Shinzato Y, Morinaga M. Phase stability change with Zr content in β-type Ti–Nb alloys. Scr Mater. 2007;57(11):1000–3.

[6] Sass JO, Sellin ML, Kauertz E, Johannsen J, Weinmann M, Stenzel M, et al. Advanced Ti–Nb–Ta alloys for bone implants with improved functionality. J Funct Biomater. 2024;15(2):46. doi: 10.3390/jfb15020046.

[7] Li Y, Yang C, Zhao H, Qu Y, Li X, Li Y. New developments of Ti-based alloys for biomedical applications. Materials. 2014;7:1709–800.

[8] Sherif ESM, Ragab SA, Abdo HS. Role of vanadium additions on the corrosion mitigation of Ti-6Al-xV alloy in simulated body fluid. Metals. 2020;10:903. doi: 10.3390/met10070903.

[9] Dai N, Zhang LZ, Zhang J, Chen Q, Wu M. Corrosion behavior of selective laser melted Ti-6Al-4 V alloy in NaCl solution. Corros Sci. 2016;102:484–9.

[10] Chong Y, Bhattacharjee T, Tsuji N. Bi-lamellar microstructure in Ti–6Al–4V: Microstructure evolution and mechanical properties. Mater Sci Eng A. 2019;762:138077.

[11] Dai N, Zhang LZ, Zhang J, Chen Q, Wu M, Yang C. Distinction in corrosion resistance of selective laser melted Ti-6Al-4Valloy on different planes. Corros Sci. 2016;111:703–10.

[12] Abdo HS, Sherif ESM, El-Serehy HA. Manufacturing of Ti-6%Al and Ti-6%Al-4%V alloys and their corrosion in sodium chloride solutions. Crystals. 2020;10:181. doi: 10.3390/cryst10030181.

[13] Krawiec H, Vignal V, Loch J, Erazmus-Vignal P. Influence of plastic deformation on the microstructure and corrosion behaviour of Ti–10Mo–4Zr and Ti–6Al–4V alloys in the Ringer's solution at 37°C. Corros Sci. 2015;96:160–70.

[14] Kawahara M, Kato-Negishi M. Link between aluminum and the pathogenesis of alzheimer's disease: the integration of the aluminum and amyloid cascade hypotheses. Int J Alzheimer's Dis. 2011;2011:276393.

[15] Kandimalla R, Vallamkondu J, Corigat EB, Gill KD. Understanding aspects of aluminum exposure in alzheimer's disease development. Brain Pathol. 2016;26:139–54.

[16] Correa DRN, Kuroda PAB, Lourenço ML, Buzalaf MAR, Grandini CR. Adjustment of the microstructure and selected mechanical properties of biomedical Ti-15Zr-Mo alloys through oxygen doping. J Alloys Compd. 2019;775:158–67.

[17] da Silva MR, Gargarella P, Plaine AH, Contieri RJ, Pauly S, Kühn U, et al. Influence of the deformation rate on phase stability and mechanical properties of a Ti–29Nb–13Ta–4.6 Zr–xO alloy analyzed by in situ high-energy X-ray diffraction during compression tests. J Mater Res. 2020;35(14):1777–89.

[18] Wu CT, Chang HT, Wu CY, Chen SW, Huang SY, Huang M, et al. Machine learning recommends affordable new Ti alloy with bone-like modulus. Materialstoday. 2020;34:41–50.

[19] Bernhard N, Berner S, De Wild M, Wieland M. The binary TiZr alloy – A newly developed Ti alloy for use in dental implants. Forum Implantol. 2009;5:30–9.

[20] Grandin HM, Berner S, Dard M. A review of titanium zirconium (TiZr) alloys for use in endosseous dental implants. Materials. 2012;5:1348–60.

[21] Lin J, Ozan S, Li Y, Ping D, Tong X, Li G, Wen C. Novel Ti-Ta-Hf-Zr alloys with promising mechanical properties for prospective stent applications. Sci Rep. 2016;6:1–11.

[22] Ijaz MF, Alharbi HF, Bahri YA, Sherif ESM. Alloy design and fabrication of duplex titanium-based alloys by spark plasma sintering for biomedical implant applications. Mater. 2022;15:8562.

[23] Samuel SG. Titanium – The material of choice? Periodontol 2000. Jun 1998;17:7–21. doi: 10.1111/j.1600-0757.1998.tb00119.x.

[24] Vannoort R. Titanium – The implant material of today. J Mater Sci. 1987;22:3801–11.

[25] Williams DF. Titanium for medical applications. In: Brunette D, Tengvall P, Textor M, Thomson P, editors. Titanium in Medicine. Berlin, Germany: Springer; 2001. p. 14–24.

[26] Hu QM, Hao SJ, Yang YL, Johansson R, Vitos B, L. Phase stability and elastic modulus of Ti alloys containing Nb, Zr, and/or Sn from first-principles calculations. Appl Phys Lett. 2008;93:121902.

[27] Kim J, Park HW. Influence of a large pulsed electron beam (LPEB) on the corrosion resistance of Ti6Al7Nb alloys. Corros Sci. 2015;96:153–60.

[28] Tahara M, Kim HY, Hosoda H, Miyazaki S. Cyclic deformation behavior of a Ti-26 at.% Nb alloy. Acta Mater. 2009;57:2461–9.

[29] Stenlund P, Omar O, Brohede U, Norgren S, Norlindh B, Johansson A, et al. Bone response to a novel Ti-Ta-Nb-Zr alloy. Acta Biomater. 2015;20:165–75.

[30] Kurtz MA, Wessinger AC, Mace A, Moreno-Reyes A, Gilbert JL. Additively manufactured Ti-29Nb-21Zr shows improved oxide polarization resistance versus Ti-6Al-4V in inflammatory simulating solution. J Biomed Mater Res. 2023;111:1538–53.

[31] Mohan L, Anandan C, Rajendran N. Electrochemical behavior and effect of heat treatment on morphology, crystalline structure of self-organized TiO_2 nanotube arrays on Ti–6Al–7Nb for biomedical applications. Mater Sci Eng C. 2015;50:394–401.

[32] Fojt J, Joska L, Malek J. Corrosion behaviour of porous Ti–39Nb alloy for biomedical applications. Corros Sci. 2013;71:78–83.

[33] Ammar HR, Sherif ESM, Sivasankaran S, Almufadi FA, Mekky AbH. Developing improved corrosion-resistant AA5083—BN/WC composites for tribological applications. Mater. 2023;16:1663. doi: 10.3390/ma16041663.

[34] Alshammri GA, Fathy N, Al-Shomar SM, Alshammari AH, Sherif ESM, Ramadan M. Effect of Al_2O_3 and NiO Nanoparticle additions on the structure and corrosion behavior of Sn – 4% Zn alloy coating carbon steel. Sustainability. 2023;15:2511. doi: 10.3390/su15032511.

[35] Sivasankaran S, Sherif ESM, Ammar HR, Alaboodi AS, Mekky AbH. Influence of oxide dispersions (Al_2O_3, TiO_2, and Y_2O_3) in CrFeCuMnNi high-entropy alloy on microstructural changes and corrosion resistance. Crystals. 2023;13:605. doi: 10.3390/cryst13040605.
[36] Alharthi N, Sherif ESM, Abdo HS, Alharbi HF, Misiolek WZ. Effect of extrusion welding locations on the corrosion of AM30 alloy extrudate. J Mater Res Technol. 2019;8:2280–9. doi: 10.1016/j.jmrt.2019.03.008.
[37] Sherif ESM, Park SM. Effects of 1,4-naphthoquinone on aluminum corrosion in 0.50 M sodium chloride solutions. Electrochim Acta. 2006;51:1313–21. doi: 10.1016/j.electacta.2005.06.018.
[38] Sherif ESM, Potgieter JH, Comins JD, Cornish L, Olubambi PA, Machio CN. The beneficial effect of ruthenium additions on the passivation of duplex stainless-steel corrosion in sodium chloride solutions. Corros Sci. 2009;51:1364–71.
[39] Latief FH, Sherif ESM, Almajid AA, Junaedi H. Fabrication of exfoliated graphite nanoplatelets-reinforced aluminum composites and evaluating their mechanical properties and corrosion behavior. J Anal Appl Pyrol. 2011;92:485–92.
[40] Sherif ESM, Bahri YA, Alharbi HF, Ijaz MF. Corrosion passivation in simulated body fluid of Ti-Zr-Ta-xSn alloys as biomedical materials. Materials. 2023;16:4603. doi: 10.3390/ma16134603.
[41] Afzali P, Ghomashchi R, Oskouei RH. On the corrosion Behaviour of low modulus titanium alloys for medical implant applications: A review. Metals. 2019;9:878.
[42] Sherif ESM, Abdo HS, Latief FH, Alharthi NH, Zein El Abedin S. Fabrication of Ti–Al–Cu new alloys by inductive sintering, characterization, and corrosion evaluation. J Mater Res Technol. 2019;8:4302–11. doi: 10.1016/j.jmrt.2019.07.040.
[43] Alam MA, Samad UA, Seikh A, Mohammed JA, Al-Zahrani SM, Sherif ESM. Development and characterization of PA 450 and PA 3282 epoxy coatings as anti-corrosion materials for offshore applications. Mater. 2022;15:2562. doi: 10.3390/ma15072562.
[44] Alam MA, Samad UA, Anis A, Sherif ESM, Abdo HS, Al-Zahrani SM. The effect of zirconia nanoparticles on thermal, mechanical, and corrosion behavior of nanocomposite epoxy coatings on steel substrates. Mater. 2023;16:4813. doi: 10.3390/ma16134813.
[45] Samad UA, Alam MA, Seikh AH, Mohammed JA, Al-Zahrani SM, Sherif ESM. Corrosion resistance performance of epoxy coatings incorporated with unmilled micro aluminium pigments. Crystals. 2023;13:558. doi: 10.3390/cryst13040558.
[46] Alam MA, Samad UA, Sherif ESM, Seikh AH, Al-Zahrani SM, Alharthi NH, et al. Synergistic effect of Ag and ZnO nanoparticles on polyaniline incorporated epoxy/2pack coatings for splash zone applications. J Coat Technol Res. 2019;16:835–45.
[47] Alam MA, Sherif ESM, Al-Zahrani SM. Mechanical properties and corrosion behavior of different coatings fabricated by diglycidyl ether of bisphenol-a epoxy resin and Aradur®-3282 curing agent. Int J Electrochem Sci. 2013;8:8388–400.